Energy Storage Materials 6 (2017) 1–8

Contents lists available at ScienceDirect

Energy Storage Materials

journal homepage: www.elsevier.com/locate/ensm

Co-embedded N-doped carbon fibers as highly efficient and binder-free cathode for Na–O_2 batteries

Jin-Ling Ma [a,b], Fan-Lu Meng [a,c], Dan Xu [a], Xin-Bo Zhang [a,*]

[a] State Key Laboratory of Rare Earth Resource Utilization Changchun Institute of Applied Chemistry, Chinese Academy of Sciences, Changchun, 130022, P.R. China

[b] University of Chinese Academy of Sciences, Beijing, 100049, P.R. China

[c] Key Laboratory of Automobile Materials (Jilin University), Ministry of Education, Department of Materials Science and Engineering, Jilin University, Changchun, 130022, China

ARTICLE INFO

Article history:
Received 8 June 2016
Received in revised form
11 September 2016
Accepted 12 September 2016
Available online 13 September 2016

Keywords:
Sodium-oxygen batteries
Cathode
Binder-free
Poor crystalline
Film-like Na_2O_2

ABSTRACT

High energy density Na-O_2 batteries is very promising for large scale energy storage, wherein the critical bottleneck lies in poor energy efficiency and cycle stability stemming from low catalytic activity and unstable structure of cathode. Herein, we propose a highly effective strategy to activate and stabilize low cost while inefficient N-doped carbon fibers by in situ simultaneous Co embedding/coating. Unexpectedly, the obtained binder-free cathode endows Na-O_2 battery with superior electrochemical performances, including low charge overpotential, high specific capacity, and especially good cycle stability, which could be attributed to the combined advantages associated with facilitated electron and mass transportation due to fiber shape and binder-free and porous structure, high conductivity and catalytic activity derived from the synergy between N-doped carbon fibers and Co (metallic and partially oxidized Co) as well as the successful tailor of the morphology of discharge products.

1. Introduction

The pressing large-scale shift from the conventional internal combustion engines to electricity driven vehicles (EVs) for alleviating environment crisis closely relies on high energy density rechargeable batteries, especially Li-O_2 cell instead of the existing lithium-ion batteries whose energy density is less than one eighth of the former even the theoretical limited of current electrode materials are reached [1–5]. However, large charge overpotential (>1 V) in Li-O_2 cell limits its cycle life to less than 100 cycles [6]. Moreover, Urgent concerns about limited reserve and distribution of lithium resources have led to an increasing interest in replacing lithium with sodium from a viewpoint of sustainability [7–9]. Unexpectedly, Na-O_2 cells demonstrate lower charge overpotential (<0.2 V) which may result in better cyclic performance and high energy efficiency than LABs [10,11]. Nevertheless, Na-O_2 cells are in their infant stage and very similar to Li-O_2 ones when thermodynamically stable sodium peroxide (Na_2O_2) dominates the discharge product derived from inevitably chemical and electrochemical transformation of the initial formed NaO_2 in a short time under glyme-based electrolyte that results in short cycle life, poor rate capability, low energy efficiency [12,13]. Therefore, the properties of the cathode material are crucial in determining the battery performance. While during the fabrication of conventional cathode, the necessary addition of inactive, insulating, and especially instable (not inert to the superoxide and peroxide from discharge) polymeric binders would severely impede efforts to improve performances of Na-O_2 batteries [14,15]. Therefore, development of highly efficient and binder-free cathode is urgently desirable but still very challenging before searching for a stable electrolyte system for Na-O_2 cell.

One-dimensional (1D) carbon materials, for example carbon fibers, have been proposed as electrocatalysts for cathode in metal-air batteries (MABs) due to the large surface to volume ratio, continuous conducting pathways for electrons, and facile strain relaxation without deformation during batteries operation [16,17]. In addition, heteroatoms, including N, B and P, doping has been employed to further introduce more catalytic active sites for pristine 1D carbon materials; [18–21]. Recent studies disclosed that nitrogen-doped graphene showed lower overpotential, higher capacity and longer cycle life compared with graphene cathode in Na-O_2 batteries [22,23]. As we all know, CoO_x always exhibits superior catalytic activity towards oxygen reduction reaction (ORR) and oxygen evolution reaction (OER) compared with other transition metal oxides in MABs [24]. However, transition metal

* Corresponding author.
E-mail address: xbzhang@ciac.ac.cn (X.-B. Zhang).

http://dx.doi.org/10.1016/j.ensm.2016.09.002
2405-8297/

oxides always present low electronic conductivity, and thus would compromise the improvement of electrochemical performance of batteries such as rate capability, especially when the discharge product is insoluble and insulated in MABs including Na-O_2 batteries, regardless of the improved catalytic activity [25,26]. In response, addition of transition metals (TMs) particles could improve the conductivity, while simply mixing or growing metal particles on the surface of 1D carbon materials cannot avoid the oxidation, aggregation and detachment of metal particles, which would decrease the conductivity and activity, respectively. Alternatively, embedding and coating transition metal into N-doped carbon fibers could further increase the conductivity and improve the catalytic activity of 1D carbon materials while avoiding the aggregating and detachment of metal particles, thus guaranteeing the stability of active sites [27,28]. Conventional methods to both encapsulate and coat metal particles into carbon fibers hold more or less drawbacks such as requirement of special equipment and multistep time- and energy-intensive procedures and are difficult in obtaining self-standing structure [27,29]. Therefore, development of new strategy to effectively fabricate self-standing TMs embedding/coating N-doped carbon fibers in a time-and cost-effective manner to significantly improve the electrochemical performances of MABs is urgently required.

Herein, as a proof-of-concept experiment, we propose and demonstrate a highly effective strategy (preparing carbon fibers, in situ N-doping, Co embedding and coating) to fabricate binder-free N-doped carbon fibers (NCFs) in situ embedded and coated with Co using an scalable coaxial electrospinning technique. Unexpectedly, when the as-obtained Co-embedding/coating N-doped carbon fibers (Co-ECNCFs) are employed as an novel binder-free cathode for Na-O_2 batteries, superior electrochemical performances, including low charge overpotential (reduced by 200 mV), high discharge capacity (increased by ~57%), and long cycle life (up to 112 cycles), are successfully obtained compared with that of NCFs one.

2. Materials and methods

2.1. Preparation for the cathode material

2.1.1. Co-ECNCFs

Polyacrylonitrile (PAN) solution was prepared by dissolving 0.5 g PAN in 5 mL DMF with vigorous stirring for 3 h. Polyvinylpyrrolidone (PVP) solution was prepared by dissolving 0.5 g PVP and 0.40 g $Co(NO_3)_2 \cdot 6H_2O$ in 5 mL N,N-dimethylformanide (DMF) for 3 h with vigorous stirring. After that, taking out 3 mL PVP solution mixed with PAN solution, then stir overnight. After that, the above mixture was transferred to a plastic syringe equipped with a 9-gauge metal nozzle made of stainless steel. The distance between the needle tip and the collector was fixed to 16 cm and the flow rate of the syringe pump was fixed at 0.8 mL h^{-1}. Electrospinning experiments were performed when relative air humidity was 50~60%. The voltage was conducted at 18 kV and a sprayed dense web of fibers was collected on the aluminum foil. The electrospun core-shell nanofibers performed calcination at 400 °C for 2 h at a heating rate of 5 °C min^{-1} and then the calcinated carbon fibers were carbonized at 700 °C for 1 h in argon gas to obtain Co-ECNCFs. Finally, Co-ECNCFs were punched into 12 mm in diameter as the self-standing cathode with the average mass of 0.7 mg, including Co percentage of 13.6% (ca. 0.095 mg) to test in Na-O_2 batteries.

2.1.2. NCFs

The NCFs was synthesized by the same method as the Co-ECNCFs except $Co(NO_3)_2 \cdot 6H_2O$ addition.

2.1.3. Co-ECNCFs-A

Co-ECNCFs were subject to the 0.5 M H_2SO_4 at 80 °C for 24 h to etch off the accessible cobalt nanoparticles. After that, it was washed by deionized water for three times, and then was dried at 100 °C in oven for 24 h.

2.1.4. PVP+Co

The PVP+Co sample was synthesized by the same method as the Co-ECNCFs except without adding PAN solution.

2.1.5. PAN+Co

The PAN+Co sample was synthesized by the same method as the Co-ECNCFs except without adding PVP solution.

2.1.6. Co-ECNCFs-O

Co-ECNCFs-O was obtained by calcinating Co-ECNCFs sample in muffle furnace at 250 °C for 4 h.

2.2. The assembly of Na-O_2 batteries

All cathodes were dried at 80 °C in vacuum oven for 24 h with the average mass of 0.7 ± 0.04 mg. For electrolyte, tetraethylene glycol dimethyl ether (TEGDME) solvent were soaked in activated molecular sieves (4 Å type) for 15 days until the water content below 10 ppm. $NaCF_3SO_3$ was heated at 80 °C in vacuum oven for 24 h. The electrolyte contains 0.5 M $NaCF_3SO_3$ in TEGDME solvent ($H_2O < 10$ ppm). All the cells were assembled using 2025-type coin cell in a glove box under argon atmosphere ($H_2O < 1$ ppm, $O_2 < 1$ ppm). Using a sodium metal foil anode ($\Phi = 10$ mm), a glass fiber separator, the above cathodes and 80 μL electrolyte were combined in sequence. The assembled cells were settled for 3 h in pure oxygen atmosphere for electrochemical measurement.

2.3. Characterization of material and discharge products

The morphologies and structures of the cathodes and discharge products were characterized by various physicochemical techniques, including XRD, SEM, TEM, XPS, FTIR and Raman spectroscopy.

2.4. Electrochemical measurement of Na-O_2 batteries

The cells were discharged to 1.6 V for the first discharge-charge under pure oxygen atmosphere. The cycling tests were controlled with the confined capacity and current density by limiting discharge cut-off potential to 1.6 V. Cyclic voltammograms (CVs) of the cells were measured between 1.9 and 4.0 V (vs. Na/Na^+) at a voltage sweep rate of 0.1 mV s^{-1}. Electrochemical impedance spectroscopy of Na-O_2 batteries was evaluated using an AC impedance analyzer within a frequency range of 10^6–10^{-2} Hz.

3. Results and discussion

The facile, mild and scalable fabrication process of the binder-free Co-ECNCFs cathode is illustrated in Fig. 1a. In brief, $Co(NO_3)_2$ is first dispersed into PVP solution for Co^{2+} bonded to oxygen atom of PVP via coordinate or covalent bonds. Then, PAN solution is added and continuous (PVP) and discontinuous (PAN) phases are obtained due to the incompatibility of the two polymers, which are then electrospun to obtain Co-ion-contained core–shell (PAN-PVP) nanofibers. Finally, the as-prepared nanofibers are carbonized at 700 °C in argon (Ar) atmosphere to obtain the binder-free Co-ECNCFs cathode for Na-O_2 batteries.

The evolution of morphology and structure of the Co-ECNCFs is investigated by scanning electron microscopy (SEM) and

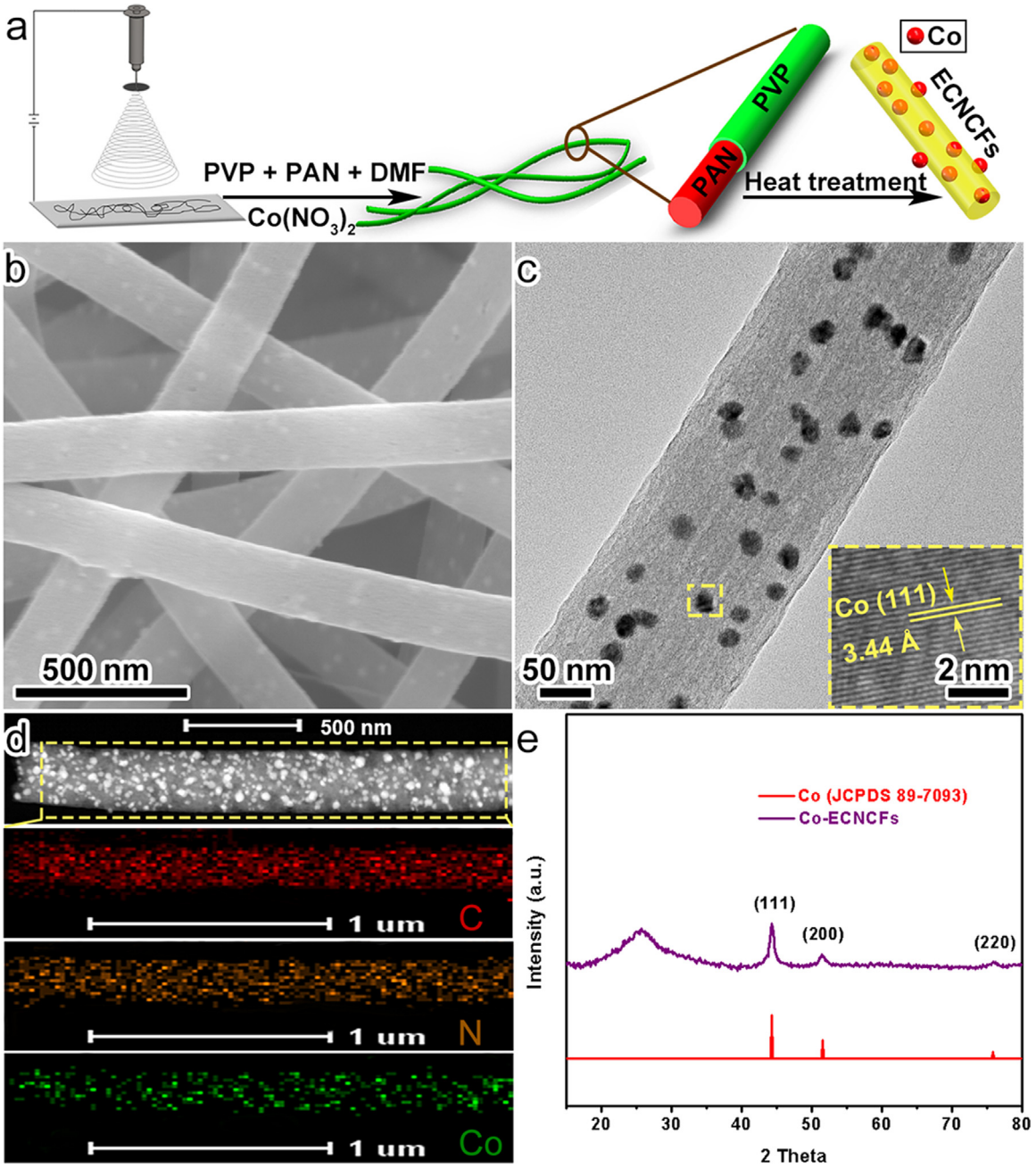

Fig. 1. Schematic illustration of the synthesis (a), SEM (b), TEM (c) (inset: HRTEM image and the (110) lattice plane of Co particles), and element mapping (d) images, and XRD pattern (e) of Co-ECNCFs.

transmission electron microscopy (TEM) techniques. As shown in Fig. 1b, the obtained Co-ECNCFs are fiber in shape with rather smooth surface, and interpenetrate to form a porous network, which could facilitate transportation of electron and oxygen as well as electrolyte. The average diameter of Co-ECNCFs is ca. 130 nm, which is smaller than that before calcination (Supplementary information, Fig. S1), and also the core-shell structure (Supplementary information, Fig. S1b–c) disappears after carbonization (Fig. 1c). The dark particles with the size range from 10∼15 nm in TEM image could be assigned to Co particles, which is consolidated by the high-magnification TEM image, wherein the d-spacing is found to be 0.34 ± 0.05 Å, corresponding to the (111) plane of metallic Co (Fig. 1c inset). Element mapping analysis demonstrates the uniform distribution of C, N, and Co elements of Co-ECNCFs (Fig. 1d). X-ray diffraction pattern (XRD) profile reveals that aside from graphite peaks, all diffraction peaks centered at 44.2, 51.5 and 75.8 degree can be indexed to the (111), (200), and (220) planes of cubic Co phase (JCPDS 89-7093) (Fig. 1e). Furthermore, in order to figure out position of Co particles in NCFs, Co-ECNCFs sample is then immersed in 0.5 M H_2SO_4 for 24 h (Co-ECNCFs-A) to remove accessible Co species [30]. The intensity of Co signal on Co-ECNCFs-A becomes weaker than that on Co-ECNCFs in Raman spectra, manifesting the elimination of outer Co (Supplementary information, Fig. S2). TEM images show some holes on the surface of Co-ECNCFs-A derived from etched Co particles, while some remaining cobalt particles can also be clearly found (Supplementary information, Fig. S3), indicating that Co particles not only anchor on the surface but also embed in the fibers of Co-ECNCFs, wherein the encapsulated Co particles could improve the electronic conductivity and tune the electronic structure of NCFs, while the exposed ones could also employed as catalytic active sites for ORR and OER. X-ray photoelectron

spectroscopy (XPS) is then employed to analyse chemical composition of Co-ECNCFs and its counterpart NCFs. It can be found that catalytic active pyridinic-N (398.3 ± 0.1 eV) and graphitic-N (401.0 ± 0.1 eV) exist for these samples with approximately 5% of the N content (Supplementary information, Fig. S4).

Another important property of the obtained Co-ECNCFs is self-standing, which could avoid the addition of instable and inactive polymer binder, and thus could be straightforwardly used as cathode for Na-O_2 batteries. It should be noted that binder-free cathode cannot be obtained when using only one of the two polymers, either PVP or PAN, bonded with Co precursor under similar synthetic conditions (Supplementary information, Fig. S5c–d). Even though the two polymers are used to prepare nitrogen-doped carbon nanofiber without Co precursor addition, self-standing NCFs cathode is easy to frangible even upon gentle bending (Supplementary information, Fig. S5a–b and 7–8), showing the power and efficiency of our proposed strategy for the fabrication of binder-free Co-ECNCFs cathode.

The electrochemical performances of binder-free Co-ECNCFs cathode are examined in Na-O_2 batteries in comparison with Co-ECNCFs-A and NCFs counterparts. Tetraethylene glycol dimethyl ether is employed as electrolyte solvent due to its relatively high stability compared with carbonate-based electrolytes [31–33]. Fig. 2a exhibits the first discharge-charge profiles of Co-ECNCFs, Co-ECNCFs-A and NCFs cathodes at a current of 250 mA g^{-1} with the cut-off discharge potential at 1.6 V (the applied current density and capacity in this work are based on the total mass of the cathode) and subsequent full charging. Interestingly, the discharge voltage of Na-O_2 batteries with Co-ECNCFs cathode is ca. 2.23 V, which is apparently higher than those of Na-O_2 batteries with the

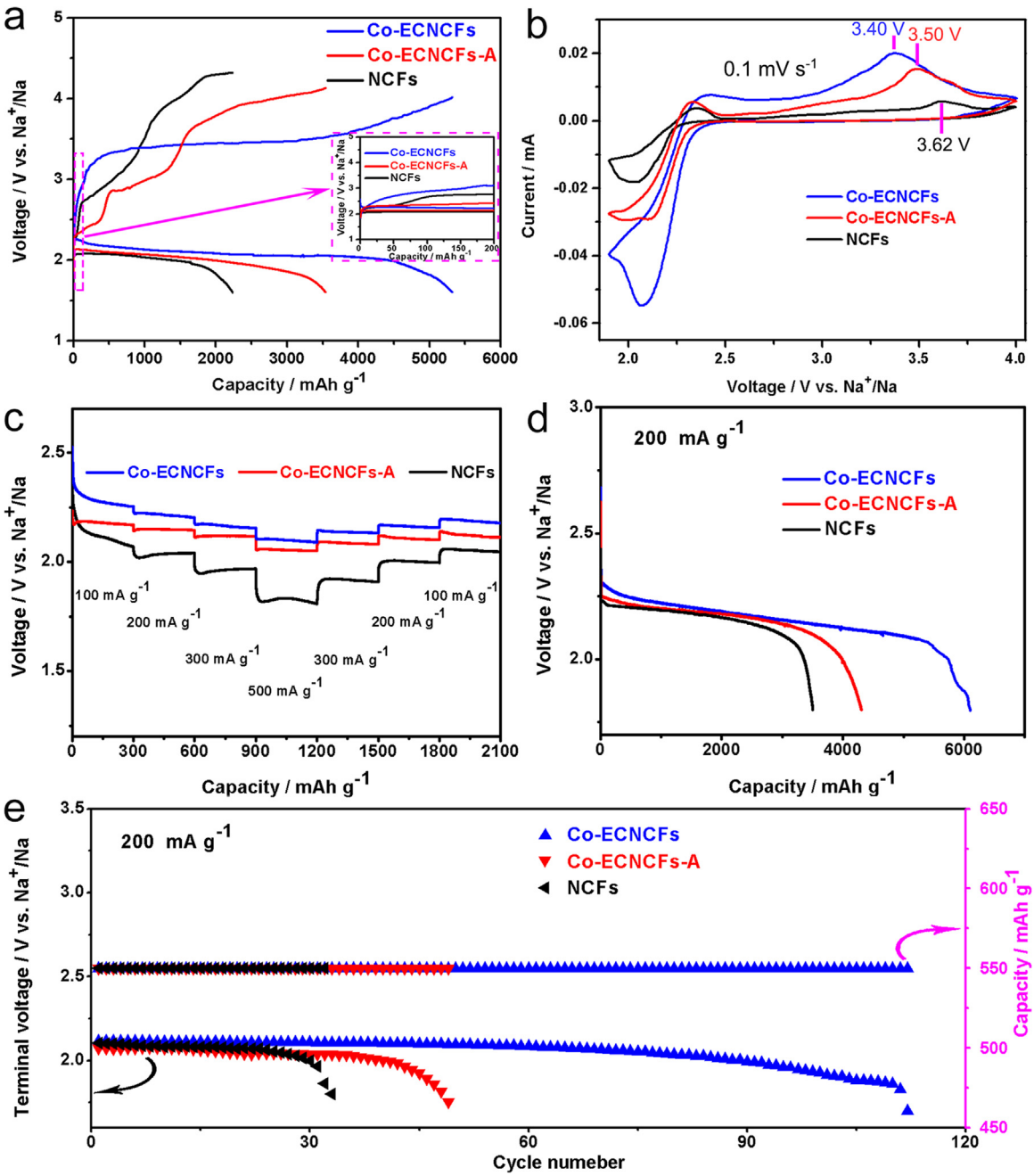

Fig. 2. First discharge-charge curves by confining discharge cut-off potential to 1.6 V (a), CV profiles at voltage sweep rate of 0.1 mV s^{-1} (b), rate performance (c), discharge capacity (d), and voltage of the terminal discharge vs. the cycle number (e) for Na-O_2 batteries with Co-ECNCFs, Co-ECNCFs-A, and NCFs electrodes.

Co-ECNCFs-A and NCFs ones. More importantly, the charge voltage of Na-O_2 batteries with Co-ECNCFs cathode rise slowly without a short low charge potential region at initial state (insert in Fig. 2a), possibly corresponding to the NaO_2 decomposition, which is contrary to those with Co-ECNCFs-A and NCFs cathodes. This discrepancy may be caused by the different catalytic mechanism caused by these cathodes and will be discussed later. Fig. 2b shows the cyclic voltammogram profiles of the three cathodes in Na–O_2 batteries [23,34]. we can see that the anodic peak (corresponding to OER) of the Co-ECNCFs cathode is 3.40 V, corresponding to negative shift of 0.10 and 0.22 V than those of the Co-ECNCFs-A (3.50 V) and the NCFs (3.62 V) cathodes, respectively, manifesting the superior catalytic activity of Co-ECNCFs cathode.

Furthermore, Na-O_2 batteries with Co-ECNCFs cathodes hold higher discharge potential than those with Co-ECNCFs-A and NCFs counterparts under all tested current densities (Fig. 2c). Additionally, Co-ECNCFs cathode also delivers much higher discharge specific capacity (6102 mAh g^{-1}) at the current density of 200 mAh g^{-1} even though its lower surface areas than that of Co-ECNCFs-A (Figs. 2d and S9). In order to exclude the electrochemical contribution from the Na^+ intercalation into carbon-based cathode, the discharge capacity with the three cathodes in Na-O_2 batteries is also examined under Ar atmosphere (Supplementary information, Fig. S10). Obviously, the capacity from Na^+ intercalation into the three cathodes can be neglected within the testing voltage window. The discharge-charge curves of Na-O_2 cell with Co-ECNCFs at current density of 200 mAg^{-1} with cut-off potentials from 1.6 to 4.4 V demonstrated that deep discharge was unbeneficial for long cycle, possibly due to the excessive accumulation of discharge products (Supplementary information, Fig. S11), so the cycling performances of the Na-O_2 batteries were tested under the current density of 200 mAg^{-1} and a fixed capacity of 550 mAh g^{-1} (Fig. 2e and S12). It can be easily found that, with the help of Co-ECNCFs cathode, 112 cycles can be obtained, which is much better than those with the Co-ECNCFs-A (49 cycles) and the NCFs (33 cycles) cathodes, and also stands as the best cycle life compared with ever reported results [34,35], highlighting the superior rechargeability of the Na-O_2 batteries with the aid of Co-ECNCFs cathode (Supplementary information, Table S1). As for the failure of the cell after 112 cycles, we attributed it to short circuit caused by the over-accumulation side products on cathode and the severe corrosion of the anode (Supplementary information, Fig. S13).

Inspired by the above obtained superior electrochemical performances of Na-O_2 batteries with Co-ECNCFs cathode, we then investigate the discharge products using various physical and chemical methods. SEM image clearly shows that film-like discharge products are deposited and uniformly coat on each carbon fibers of Co-ECNCFs cathode, which could effectively utilize the surface area of the cathode, thus improving discharge capacity (Fig. 3a) [34,36], in sharp contrast with the other two cathodes, wherein the discharge products are aggregated particles (Fig. 3b and c). This fully explains the higher discharge capacity of Co-ECNCFs cathode achieved in spite of its relatively lower surface areas. The homogeneous formation of film-like product might be attributed to the embedded cobalt particles inside carbon matrix, which could serve as electron-deficient position and change the electron distribution in nearby carbons and the interaction between oxygen and the metal/carbon hybrids, favoring film-like discharge products formation. The discharge products on the three cathodes after discharged to 1.8 V are further characterized by XRD (Fig. 3d). Obviously, poor crystallinity Na_2O_2 with broader and less intense XRD pattern are the dominated discharged products on Co-ECNCFs cathode while crystallinity $Na_2O_2 \cdot 2H_2O$ occurs in the

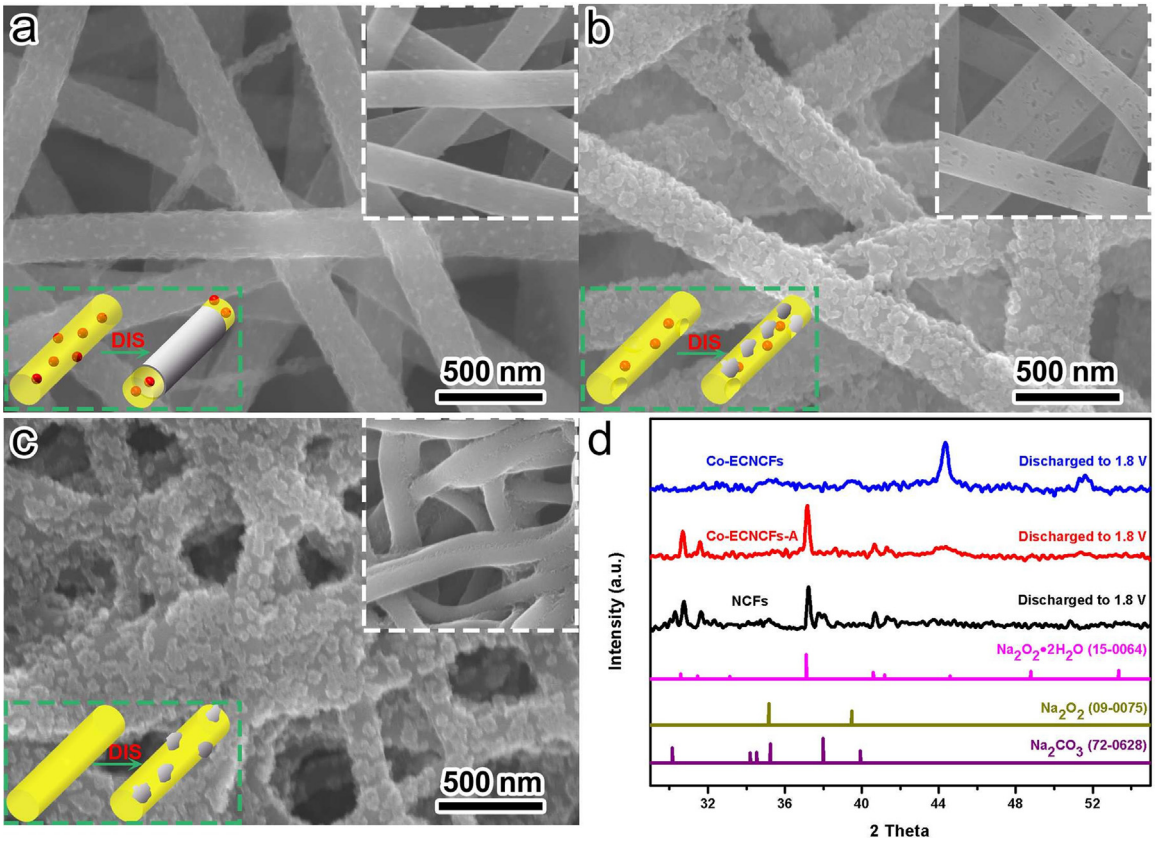

Fig. 3. SEM images of discharge products on Co-ECNCFs (a), Co-ECNCFs-A (b), and NCFs (c) cathodes (inset: pristine cathode and scheme of change of the corresponding cathode), XRD patterns of discharge products on the three cathodes (d).

Co-ECNCFs-A and NCFs, possibly as a result of the dissolution and ionization of the formed sodium superoxide, liberating superoxide anion and triggering the formation of $Na_2O_2 \cdot 2H_2O$ as ever reported [37], which would incur large polarization upon charging. Some Na_2CO_3 are observed on NCFs likely due to the instability of NCFs cathode. These results are consistent with the Raman results (Supplementary information, Fig. S14). It is reported that poor crystalline discharge products are rich of defects and can be decomposed with less energy, thus resulting in low charge potential [38–40], which is in good consistent with electrochemical performances in terms of charge potential (Fig. 2a and b). The different discharge products between Co-ECNCFs and the other two cathodes may originate from the different catalysis mechanism: two-electron reaction toward ORR on Co-ECNCFs cathode may preferentially occur while for Co-ECNCFs-A and NCFs ones, one-electron reaction dominates and generates NaO_2 with subsequent chemical and electrochemical transformation to $Na_2O_2 \cdot 2H_2O$, even though the reason for this at present is unclear in Na-O_2 system [32,41]. This hypothesis can be confirmed by the galvanostatic intermittent titration technique (GITT) test [42,43], from which equilibrium voltage (Ueq) located at 2.31 V associated with the formation of Na_2O_2 with Co-ECNCFs cathode, while it located at 2.20 V corresponding to the formation of NaO_2 with the other two cathodes (Supplementary information, Fig. S15). Besides, no short low charging potential profile corresponding to decomposition NaO_2 appears on Co-ECNCFs cathode which is contrast with the other two cathodes. To evaluate the reversibility of the discharge products, Fourier transform infrared spectroscopy (FTIR) measurement are employed [44]. Two characteristic peaks (879 and 1442 cm^{-1}) of Na_2O_2 can be observed in FTIR spectra and disappear after charge process while recover after discharge process, showing the good reversibility of the discharge product, Na_2O_2 (Supplementary information, Fig. S16). The long-term stability of discharge products was analyzed by ultraviolet visible (UV–vis) spectroscopy and XRD and results demonstrated that Na_2O_2 was reducing with cycling by reduced the intensity of Na_2O_2 in XRD and extinction of the $TiOSO_4$ solutions caused by H_2O_2 derived from Na_2O_2 reacting with H_2O (Supplementary information, Fig. S17 and 18), manifesting the instability of Na_2O_2 in long term cycling. This may result from isolated and undecomposed product deposited on cathode, causing low charge transfer efficiency for Na_2O_2 formation.

The electrochemical impedance spectra (EIS) of Na–O_2 batteries at different discharge/charge stages are tested to understand the above obtained difference in electrochemical performances (Supplementary information, Fig. S19). Before discharge, Na-O_2 battery with Co-ECNCFs cathode holds the lowest charge-transfer resistance (Rct) corresponding to the depressed semicircle in the Nyquist plot at high frequencies, which might be attributed to the high conductivity of Co-ECNCFs cathode. After the first discharge, the Rct of all the three batteries increases (Supplementary information, Fig. S19b), which is due to the poor electronic conductive of discharge product (Na_2O_2) generated on cathode. Interestingly, even after the first (1st) and fifth (5th) charging, the Rct of Na-O_2 batteries with Co-ECNCFs is still lower than those with Co-ECNCFs-A and NCFs counterparts which could be responsible for the improved cycling performance of Na-O_2 batteries with Co-ECNCFs cathode.

To gain deep insight into underlying catalytic mechanism concerning Co-ECNCFs cathode in Na-O_2 batteries, the chemical states of Co in Co-ECNCFs cathode have been investigated. XPS results show that the characteristic peak of metallic Co (778.0 eV) gradually disappears and only those of CoO_x exist owing to oxidation of cobalt during charging (Fig. 4a). However, no crystalline phase of CoO_x can be found in XRD even after the 30th charging, indicating that the in situ formed CoO_x layer is very thin and/or weak in crystallinity (Fig. 4b). HRTEM results show oxidation of Co layer with cycling to reach a maximum thickness of 5–6 nm oxidized layer at the 5th cycles (Fig. 4c–h) with subsequent invariability. This is also confirmed by vibrating sample magnetometer method, [45–47] wherein magnetic moment of the pristine cathode is 34.6 emu g^{-1}, which reduces to 26.6 emu g^{-1} at the 5th cycles with subsequent stability as shown in Supplementary information, Fig. S20. Based on the above obtained results, it can be concluded that a very small portion of naked Co is oxidized during robust electrochemical conditions to form a thin layer of CoO_x for OER, and the large fraction of embedded Co are free of oxidization due to the protective layer of formed CoO_x, thus enhancing the conductivity of the in-situ formed insulated CoO_x for high efficiency of electron transfer and formation of the uniform distribution film-like discharge products. On the other hand, the

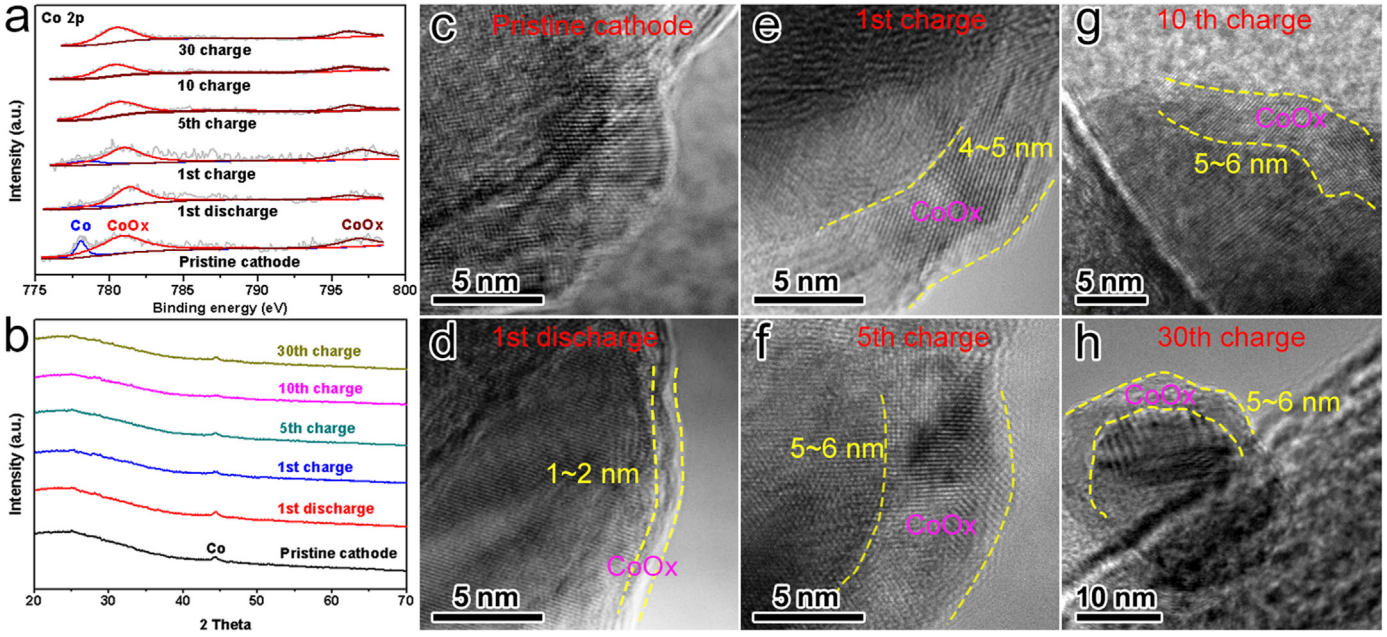

Fig. 4. High-resolution Co2p spectra (a), XRD pattern (b), and the corresponding HRTEM images of exposed cobalt on the Co-ECNCFs cathode (c–h).

formed stable CoO_x active sites derived from chemical and electrochemical oxidation also play a great role on long cycling [48]. All these explain the superior catalytic activity of the Co-ECNCFs cathode compared with Co-ECNCFs-A and NCFs counterparts in Na-O_2 batteries. For the sake of proving our speculation, Co-ECNCFs cathode with complete oxidization by heat treatment in a muffle furnace (Co-ECNCFs-O) is also prepared to examine in Na-O_2 batteries, which presents high charge potential due to the low intrinsic conductivity of Co oxides, thus amplifying inner resistance and incurred limited cycle number caused by high charge potential (Supplementary information, Fig. S21–22 and Table S2).

4. Conclusions

In conclusion, as a proof-of-concept experiment, a facile strategy has been proposed to activate and integrate the carbon fibers cathodes by in situ N-doping as well as Co embedding and coating towards a highly efficient and robust Co-ECNCFs cathode for Na-O_2 batteries, using a facile, mild, and scalable technique. Surprisedly, when first employed as novel cathode for Na-O_2 batteries, superior electrochemical performances, including high discharge capacity (increased by $\sim$ 57%), low charge overpotential (reduced by 200 mV), and especially long cycle life (up to 112 cycles), are successfully obtained, which stems from the tailored properties of Co-ECNCFs cathode, accelerated transportation of mass and electron due to fiber shape and binder-free and porous structure, improved and stabilized kinetics of ORR/OER derived from the synergy between N-doping and Co (metallic and partially oxidized Co) encapsulating/coating as well as the successful tailor of the morphology of discharge product. We anticipate this strategy will form the basis for an unprecedented perspective in the development of high-performing cathode for next generation Na-O_2 batteries.

Note

The authors declare no competing financial interest.

Acknowledgements

This work was financially supported by the National Program on Key Basic Research Project of China (973 Program, Grant nos. 2012CB215500 and 2014CB932300), and the National Natural Science Foundation of China (Grant nos. 21101147, 21203176, and 51301160).

Appendix A. Supplementary material

Supplementary data associated with this article can be found in the online version at http://dx.doi.org/10.1016/j.ensm.2016.09.002.

References

[1] K.M. Abraham, Z. Jiang, A polymer electrolyte-based rechargeable lithium/oxygen battery, J. Electrochem. Soc. 143 (1996) 1–5.
[2] E. Peled, D. Golodnitsky, H. Mazor, M. Goor, S. Avshalomov, Parameter analysis of a practical lithium- and sodium-air electric vehicle battery, J. Power Sources 196 (2011) 6835–6840.
[3] E. Peled, D. Golodnitsky, R. Hadar, H. Mazor, M. Goor, L. Burstein, Challenges and obstacles in the development of sodium-air batteries, J. Power Sources 244 (2013) 771–776.
[4] J.-J. Xu, Z.-L. Wang, D. Xu, L.-L. Zhang, X.-B. Zhang, Tailoring deposition and morphology of discharge products towards high-rate and long-life lithium-oxygen batteries, Nat. Commun. 4 (2013) 2438.
[5] P.G. Bruce, S.A. Freunberger, L.J. Hardwick, J.-M. Tarascon, Li-O_2 and Li-S batteries with high energy storage, Nat. Mater. 11 (2012) 19–29.
[6] Z. Peng, S.A. Freunberger, Y. Chen, P.G. Bruce, A reversible and higher-rate Li-O_2 battery, Science 337 (2012) 563–566.
[7] C. Zhang, H.B. Wu, C. Yuan, Z. Guo, X.W. Lou, Confining sulfur in double-shelled hollow carbon spheres for lithium-sulfur batteries, Angew. Chem. Int. Ed. 51 (2012) 9592–9595.
[8] S. Xin, L. Gu, N.-H. Zhao, Y.-X. Yin, L.-J. Zhou, Y.-G. Guo, L.-J. Wan, Smaller sulfur molecules promise better Lithium–Sulfur batteries, J. Am. Chem. Soc. 134 (2012) 18510–18513.
[9] Z. Wei Seh, W. Li, J.J. Cha, G. Zheng, Y. Yang, M.T. McDowell, P.-C. Hsu, Y. Cui, Sulphur–TiO_2 yolk-shell nanoarchitecture with internal void space for long-cycle lithium-sulphur batteries, Nat. Commun. 4 (2013) 1331.
[10] P. Hartmann, C.L. Bender, M. Vračar, A.K. Dürr, A. Garsuch, J. Janek, P. Adelhelm, A rechargeable room-temperature sodium superoxide (NaO_2) battery, Nat. Mater. 12 (2013) 228–232.
[11] B.D. McCloskey, J.M. Garcia, A.C. Luntz, Chemical and Electrochemical Differences in Nonaqueous Li-O_2 and Na-O_2 Batteries, J. Phys. Chem. Lett. 5 (2014) 1230–1235.
[12] C. Xia, R. Black, R. Fernandes, B. Adams, L.F. Nazar, The critical role of phase-transfer catalysis in aprotic sodium oxygen batteries, Nat. Chem. 7 (2015) 496–501.
[13] J. Kim, H. Park, B. Lee, W.M. Seong, H.-D. Lim, Y. Bae, H. Kim, W.K. Kim, K. H. Ryu, K. Kang, Dissolution and ionization of sodium superoxide in sodium-oxygen batteries, Nat. Commun. 7 (2016) 10670.
[14] X.-l Huang, R.-z Wang, D. Xu, Z.-l Wang, H.-g Wang, J.-j Xu, Z. Wu, Q.-c Liu, Y. Zhang, X.-b Zhang, Homogeneous CoO on Graphene for Binder-Free and Ultralong-Life Lithium Ion Batteries, Adv. Funct. Mater. 23 (2013) 4345–4353.
[15] E. Nasybulin, W. Xu, M.H. Engelhard, Z. Nie, X.S. Li, J.-G. Zhang, Stability of polymer binders in Li-O_2 batteries, J. Power Sources 243 (2013) 899–907.
[16] L. Qie, W.-M. Chen, Z.-H. Wang, Q.-G. Shao, X. Li, L.-X. Yuan, X.-L. Hu, W.-X. Zhang, Y.-H. Huang, Nitrogen-doped porous carbon nanofiber webs as anodes for lithium ion batteries with a super high capacity and rate capability, Adv. Mater. 24 (2012) 2047–2050.
[17] G. Zheng, Y. Yang, J.J. Cha, S.S. Hong, Y. Cui, Hollow carbon nanofiber-encapsulated sulfur cathodes for high specific capacity rechargeable lithium batteries, Nano Lett. 11 (2011) 4462–4467.
[18] J. Ryu, N. Jung, D.-H. Lim, D.Y. Shin, S.H. Park, H.C. Ham, J.H. Jang, H.-J. Kim, S. J. Yoo, P-modified and carbon shell coated Co nanoparticles for efficient alkaline oxygen reduction catalysis, Chem. Commun. 50 (2014) 15940–15943.
[19] W.J. Lee, U.N. Maiti, J.M. Lee, J. Lim, T.H. Han, S.O. Kim, Nitrogen-doped carbon nanotubes and graphene composite structures for energy and catalytic applications, Chem. Commun. 50 (2014) 6818–6830.
[20] Y. Zheng, Y. Jiao, L. Ge, M. Jaroniec, S.Z. Qiao, Two-step boron and nitrogen doping in graphene for enhanced synergistic catalysis, Angew. Chem. Int. Ed. 52 (2013) 3110–3116.
[21] L.-F. Chen, Z.-H. Huang, H.-W. Liang, W.-T. Yao, Z.-Y. Yu, S.-H. Yu, Flexible all-solid-state high-power supercapacitor fabricated with nitrogen-doped carbon nanofiber electrode material derived from bacterial cellulose, Energy Environ. Sci. 6 (2013) 3331–3338.
[22] W. Liu, Q. Sun, Y. Yang, J.Y. Xie, Z.W. Fu, An enhanced electrochemical performance of a sodium-air battery with graphene nanosheets as air electrode catalysts, Chem. Commun. 49 (2013) 1951–1953.
[23] Y. Li, H. Yadegari, X. Li, M.N. Banis, R. Li, X. Sun, Superior catalytic activity of nitrogen-doped graphene cathodes for high energy capacity sodium-air batteries, Chem. Commun. 49 (2013) 11731–11733.
[24] W.-H. Ryu, T.-H. Yoon, S.H. Song, S. Jeon, Y.-J. Park, I.-D. Kim, Bifunctional Composite Catalysts Using Co_3O_4 Nanofibers Immobilized on Nonoxidized Graphene Nanoflakes for High-Capacity and Long-Cycle Li–O_2 Batteries, Nano Lett. 13 (2013) 4190–4197.
[25] W.-M. Liu, W.-W. Yin, F. Ding, L. Sang, Z.-W. Fu, $NiCo_2O_4$ nanosheets supported on Ni foam for rechargeable nonaqueous sodium–air batteries, Electrochem. Commun. 45 (2014) 87–90.
[26] Z. Khan, S. Park, S.M. Hwang, J. Yang, Y. Lee, H.-K. Song, Y. Kim, H. Ko, Hierarchical urchin-shaped α-MnO_2 on graphene-coated carbon microfibers: a binder-free electrode for rechargeable aqueous Na–air battery, NPG Asia Mater. 8 (2016) e294.
[27] J. Deng, P. Ren, D. Deng, L. Yu, F. Yang, X. Bao, Highly active and durable non-precious-metal catalysts encapsulated in carbon nanotubes for hydrogen evolution reaction, Energy Environ. Sci. 7 (2014) 1919–1923.
[28] M. Tavakkoli, T. Kallio, O. Reynaud, A.G. Nasibulin, C. Johans, J. Sainio, H. Jiang, E.I. Kauppinen, K. Laasonen, Single-shell carbon-encapsulated iron nanoparticles: synthesis and high electrocatalytic activity for hydrogen evolution reaction, Angew. Chem. Int. Ed. 54 (2015) 4535–4538.
[29] G. Wu, K.L. More, C.M. Johnston, P. Zelenay, High-performance electrocatalysts for oxygen reduction derived from polyaniline, iron, and cobalt, Science 332 (2011) 443–447.
[30] X. Zou, X. Huang, A. Goswami, R. Silva, B.R. Sathe, E. Mikmeková, T. Asefa, Cobalt-embedded nitrogen-rich carbon nanotubes efficiently catalyze hydrogen evolution reaction at all pH values, Angew. Chem. Int. Ed. 53 (2014) 4372–4376.
[31] N. Zhao, X. Guo, Cell chemistry of sodium–oxygen batteries with various nonaqueous electrolytes, J. Phys. Chem. C 119 (2015) 25319–25326.
[32] J. Kim, H.-D. Lim, H. Gwon, K. Kang, Sodium-oxygen batteries with alkyl-carbonate and ether based electrolytes, Phys. Chem. Chem. Phys. 15 (2013) 3623–3629.

[33] B.D. McCloskey, D.S. Bethune, R.M. Shelby, G. Girishkumar, A.C. Luntz, Solvents' Critical Role in Nonaqueous Lithium-Oxygen Battery Electrochemistry, J. Phys. Chem. Lett. 2 (2011) 1161–1166.
[34] Q. Sun, H. Yadegari, M.N. Banis, J. Liu, B. Xiao, B. Wang, S. Lawes, X. Li, R. Li, X. Sun, Self-stacked nitrogen-doped carbon nanotubes as long-life air electrode for sodium-air batteries: Elucidating the evolution of discharge product morphology, Nano Energy 12 (2015) 698–708.
[35] Z. Jian, Y. Chen, F. Li, T. Zhang, C. Liu, H. Zhou, High capacity Na-O_2 batteries with carbon nanotube paper as binder-free air cathode, J. Power Sources 251 (2014) 466–469.
[36] H. Yadegari, M.N. Banis, B. Xiao, Q. Sun, X. Li, A. Lushington, B. Wang, R. Li, T.-K. Sham, X. Cui, X. Sun, Three-dimensional nanostructured air electrode for sodium-oxygen batteries: a mechanism study toward the cyclability of the cell, Chem. Mater. 27 (2015) 3040–3047.
[37] N. Zhao, C. Li, X. Guo, Long-life Na-O_2 batteries with high energy efficiency enabled by electrochemically splitting NaO_2 at a low overpotential, Phys. Chem. Chem. Phys. 16 (2014) 15646–15652.
[38] E. Yilmaz, C. Yogi, K. Yamanaka, T. Ohta, H.R. Byon, Promoting Formation of Noncrystalline Li_2O_2 in the Li-O_2 Battery with RuO_2 Nanoparticles, Nano Lett. 13 (2013) 4679–4684.
[39] Y. Yang, W. Liu, Y. Wang, X. Wang, L. Xiao, J. Lu, L. Zhuang, A PtRu catalyzed rechargeable oxygen electrode for Li-O_2 batteries: performance improvement through Li_2O_2 morphology control, Phys. Chem. Chem. Phys. 16 (2014) 20618–20623.
[40] F. Tian, M.D. Radin, D.J. Siegel, Enhanced charge transport in amorphous Li_2O_2, Chem. Mater. 26 (2014) 2952–2959.
[41] C.L. Bender, D. Schröder, R. Pinedo, P. Adelhelm, J. Janek, One- or two-electron transfer? the ambiguous nature of the discharge products in sodium-oxygen batteries, Angew. Chem. Int. Ed. 55 (2016) 4640–4649.
[42] B.G. Kim, H.-J. Kim, S. Back, K.W. Nam, Y. Jung, Y.-K. Han, J.W. Choi, Improved reversibility in lithium-oxygen battery: understanding elementary reactions and surface charge engineering of metal alloy catalyst, Sci. Rep. 4 (2014) 4225.
[43] Z.H. Cui, X.X. Guo, H. Li, Equilibrium voltage and overpotential variation of nonaqueous Li-O_2 batteries using the galvanostatic intermittent titration technique, Energy Environ. Sci. 8 (2015) 182–187.
[44] H. Yadegari, Y. Li, M.N. Banis, X. Li, B. Wang, Q. Sun, R. Li, T.-K. Sham, X. Cui, X. Sun, On rechargeability and reaction kinetics of sodium-air batteries, Energy Environ. Sci. 7 (2014) 3747–3757.
[45] S. Guo, S. Zhang, L. Wu, S. Sun, Co/CoO nanoparticles assembled on graphene for electrochemical reduction of oxygen, Angew. Chem. Int. Ed. 51 (2012) 11770–11773.
[46] T. Ozkaya, A. Baykal, Y. Koseoğlu, H. Kavas, Synthesis of Co_3O_4 nanoparticles by oxidation-reduction method and its magnetic characterization, Cent. Eur. J. Chem. 7 (2009) 410–414.
[47] M. Cabo, E. Pellicer, E. Rossinyol, M. Estrader, A. Lopez-Ortega, J. Nogues, O. Castell, S. Surinach, M.D. Baro, Synthesis of compositionally graded nanocast NiO/$NiCo_2O_4$/Co_3O_4 mesoporous composites with tunable magnetic properties, J. Mater. Chem. 20 (2010) 7021–7028.
[48] H.G. Tompkins, J.A. Augis, The oxidation of cobalt in air from room temperature to 467 °C, Oxid. Met. 16 (1981) 355–369.